Solid Oxide Cells for Hydrogen Generation and Usage: From Materials to Systems

Norbert H. Menzler[1], Dominik Schäfer[2], Nicolas Kruse[2], Roland Peters[2], Felix Kunz[2]

1 Forschungszentrum Jülich GmbH, Institute of Energy and Climate Research (IEK), IEK-1: Materials Synthesis and Processing, 52425 Jülich, Germany
2 Forschungszentrum Jülich GmbH, Institute of Energy and Climate Research (IEK), IEK-9: Fundamental Electrochemistry, 52425 Jülich, Germany

1. Introduction

Fuel cells directly convert chemical energy stored in a gas into electricity. The base chemical reaction is the *Knallgas* reaction, the combination of oxygen and hydrogen to form water (vapor). The opposite of this, the splitting of water into hydrogen and oxygen, is electrolysis. Fuel cells and electrolyzers can operate at different temperatures using different electrolytes and electrodes. Additionally, charge transport through the electrolyte can be achieved with different carriers, for example protons, oxygen ions, OH^- ions, or CO_3^{2-} molecules. Charge neutrality is ensured by an outer connection where electrons are diffusing, thus closing the circuit. Based on the operational temperature and the electrolyte, the fuel cells and electrolyzers used can be divided into:

- Polymer electrolyte fuel and electrolyzer cells (PEFCs, PEECs)
- Alkaline fuel and electrolyzer cells (AFCs, AECs)
- Phosphoric acid fuel cells (PAFCs)
- Molten carbonate fuel cells (MCFCs)
- Solid oxide fuel and electrolyzer cells (SOFCs, SOECs)

While PEFCs/PEECs, AFCs/AECs, and PAFCs typically operate below 100°C, MCFCs operate at ~ 650°C and SOFCs/SOECs between 600°C and 850°C. PAFCs and MCFCs only exist as fuel cells. A combination of PEECs and AECs is the anion exchange electrolysis cell (AEEC), which also operates at lower temperatures. While polymer electrolyte and alkaline fuel and electrolyzer cells cannot operate in both modes within one unit, the solid oxide cell (SOC) is able to do so. The resulting system is the reversible SOC (rSOC). The SOC typically uses oxygen ions as a charge carrier, but a variant of the SOC are the proton-conducting fuel and electrolysis cells (PCFCs/PCECs), which operate at intermediate temperatures of ~ 500°C.
In this article, we focus on the fuel and electrolyzer technologies that use a solid ceramic membrane as an electrolyte, namely the SOC and the PCC. SOFC and SOEC systems are state of the art, while PCC systems are still in the R&D phase. The article will thus be predominantly dedicated to SOCs and, where applicable, PCCs are cited.

2. Cells

High-temperature fuel and electrolyzer cells can be subdivided by their geometrical design and the layer which ensures mechanical support. From a design perspective, there are tubular, planar, and quasi-planar cells. Tube dimensions range from a length of 5 cm to 1.8 m, with diameters ranging from several millimeters to ~ 2.5 cm. Planar cells have a typical stack-ready dimension of approx. 10–15 cm in length in the x and y direction. Quasi-tubular designs are constructed as planar cells on a flat tubular support. At present, tubular designs are more commonly developed in East Asia, while planar designs are predominant in Europe and North America. In this article, we focus exclusively on planar designs.

A typical fuel/electrolyzer cell consists of at least three layers: one electrolyte and two electrodes (anode and cathode). In terms of electrochemical functionality, their thickness ranges from several to tens of micrometers, which means that one of the layers or an additional layer must assume the mechanical bearing function. All support types are available, for example cathode-, electrolyte-, and anode-supported cells. As in electrolyzer mode, the current direction is opposite to the fuel cell mode. The electrodes are now referred to as the air electrode (AE) and the fuel electrode (FE), thus making it unnecessary to name the operational mode. Three types of SOCs are predominantly used today: electrolyte-supported cells (ESCs), fuel-electrode-supported cells (FESCs), and metal-supported cells (MSCs). In MSCs, the support – a high temperature metal – has no electrochemical function except for the mechanical bearing and the electrical connection. ESCs are today used by, for example, Sunfire (GER) [1], Hexis (CHE) [2], BloomEnergy (USA) [3], IKTS (GER) [4], and Kerafol (GER) [5]. The most commonly used MSC is the one developed by CeresPower (GBR) [6], which licenses its technology to Bosch (GER) [7], Weichai (CHN) [8], and Doosan (KOR) [9]. AVL (AUT), a system integrator, also uses stacks from CeresPower [10]. The FESC has been developed by, for example, Solydera (formerly SolidPower; ITA/CHE) [11], Elcogen (EST) [12], Nexceris (USA) [13], Risoe/DTU (DNK) [14], and Forschungszentrum Jülich (GER) [15, 16].
All three types of SOCs have advantages and limitations. ESCs and FESCs were developed earlier than MSCs, which is why there are more stack and system results. In the last few years, however, the MSC has been rapidly catching up. In Figure 1, cross-sectional SEM micrographs of the three cell types are shown. The materials and structural designs of these three types are presented in the following subsections.
Before providing more details on the materials, the basic requirements of the three layers are outlined.

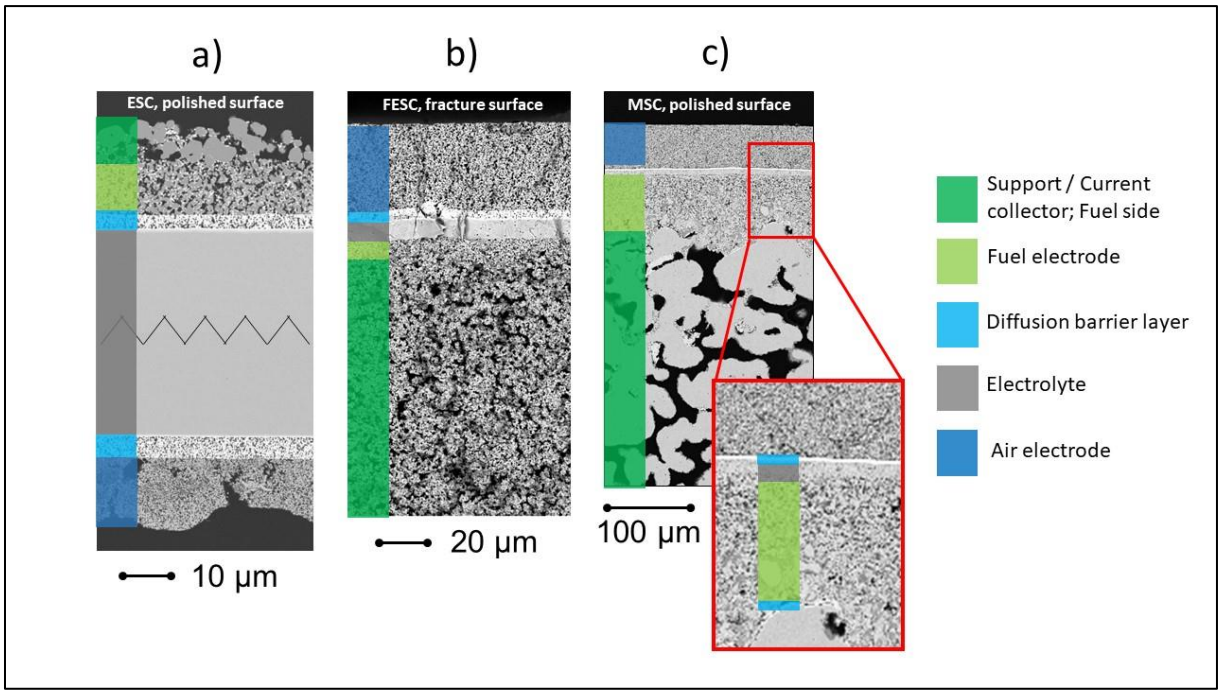

Figure 1: SEM cross sections of typical planar solid oxide cells. a) electrolyte-supported, b) fuel electrode-supported, and c) metal-supported (sample origin: a) Kerafol [5], b) Forschungszentrum Jülich, c) Plansee SE [17]). Note: photographs have different magnifications, the metering bar in c) refers to the lower magnified photo and the coloring is comparable throughout all cell types

2.1 Functional layer requirements

Electrolyte

- Gas tightness
- Chemical stability in reducing (fuel) and oxidizing (air) conditions
- Good ionic (protonic) conduction
- No electron conduction (internal short circuit)

Fuel electrode

- Porous to ensure gas phase diffusion of educts and products
- Electronic conductivity
- Ionic conductivity
- High amount of triple phase boundaries (TPBs; areas where the ion conductor, the electron conductor, and the pores meet)
- Good catalytic activity for the hydrogen/oxygen reactions
- Chemical stability in reducing environment
- CTE adapted to the electrolyte material
- No negative interaction with electrolyte material during manufacturing and operation (or incorporation of a diffusion barrier)

Air electrode

- Porous to ensure air diffusion
- Electronic conductivity
- Good ionic bulk conductivity
- Good oxygen surface adhesion and catalytic activity for oxygen splitting
- Chemical stability in oxidizing conditions
- CTE adapted to the electrolyte material
- No negative interaction with electrolyte material during manufacturing and operation (or incorporation of a diffusion barrier)

2.2 SOC types

ESC

The electrolyte-supported cell is based on a relatively thick (~ 80–150 µm) tape-cast electrolyte. Typical materials used are 3YSZ (with 3 mol% yttria-stabilized zirconia), 8YSZ (8 mol% yttria), or 10Sc1CeSZ (zirconia co-stabilized with 10 mol% scandia and 1mol% ceria). As the mechanical strength of 3YSZ is superior to that of 8YSZ, and ScSZ is relatively expensive, 3YSZ is most commonly used today, with an acceptance of its lower ionic conductivity compared to the other two variants. The two electrodes are typically screen printed on the end-sintered support and are sintered either separately at different temperatures or in parallel at a given temperature. Typical sintering temperatures are ~ 1400°C for the support and 1000–1200°C for the electrodes. A bilayer consisting of an inner electrochemically active layer and an outer current collection layer are applied as a fuel electrode. The electrode typically consists of metallic nickel as an electron conductor as well as catalytic active material and gadolinia-doped ceria (GDC) as an ion conductor and adaptor of the coefficient of thermal expansion to that of YSZ. In many cases, an additional layer composed of GDC is applied between the electrolyte and the fuel electrode. This layer can function as an adaptation layer to enhance adhesion or to suppress the bending of the YSZ electrolyte due to the requirement of a GDC coating on the air side, as explained in the following. On the air side, ceramic mixed ionic–electronic conducting (MIEC) perovskites are typically used. The basic chemical formula is ABO_3 and lanthanides (La, Pr) or earthen alkalis (Sr, Ca) are typically used at the A site and transition metal ions such as Mn, Co, and Fe are incorporated on the B site. Perovskites enable multiple doping with different elements, as their crystal structure location is typically defined by their atomic radius (either A site or B site). Stoichiometric perovskites are scarce and A-site sub-stoichiometric variants usually exist. A-site sub-stoichiometry ensures higher performance, a longer lifetime, and less susceptibility to deterioration during synthesis and manufacturing (e.g. free La would react to La_2O_3 and subsequently in air to $La(OH)_3$ followed by layer destruction due to volume

expansion). The A-site sub-stoichiometry is compensated in the lattice by oxygen vacancies. The final real chemical formula is thus $A_{1-x}B_xO_{3-\delta}$. Typical air electrodes are LSC and LSCF (La-Sr-Co and La-Sr-Co-Fe perovskite). The main drawback of both materials is their reactivity with YSZ during processing and operation. Sr from the perovskite reacts with the Zr-forming Sr zirconate, an insulating layer. The traditional way of overcoming this issue is to introduce a diffusion barrier layer. However, this additional layer must fulfill a number of requirements such as i) non-reactivity with YSZ and LSC(F), ii) ionic conductivity, and iii) the hindrance of element diffusion from both neighboring layers. The material of choice is GDC. In summary, a state-of-the-art ESC consists of a pure Ni current collector and an Ni-GDC electrode on the fuel side, a GDC barrier layer, a YSZ electrolyte, another GDC barrier layer, and an LSC(F) air electrode. The thicknesses of the barrier layer are typically 5–10 µm and those of the electrodes are 20–50 µm. All layers are sintered in ambient air, including the Ni-GDC fuel electrode. To do so, NiO is used instead of metallic Ni in production. During cell or stack start-up, the nickel oxide is reduced to Ni.

FESC

From a materials perspective, FESCs and ESCs have various similarities. This applies to the metallic Ni in the fuel electrode, the type of electrolyte, the barrier layer, and the air electrodes. Two main differences are that the electrolyte is composed of fully stabilized zirconia (8YSZ) instead of 3YSZ, and that the zirconia is also part of the fuel electrode. An FESC thus consists of a thick (250–500 µm), coarse fuel-side support composed of Ni and 8YSZ, a thin, fine-grained fuel electrode (Ni/8YSZ; d ~ 10 µm), a thin, gas-tight electrolyte (8YSZ; d ~ 10 µm), a barrier layer made of GDC (d ~ 5 µm), and an air electrode composed of LSC(F) with a thickness of around 50 µm. Typically, the support is tape cast and all subsequent layers are applied by screen printing. Alternatively, the support, the fuel electrode, and the electrolyte can be tape cast green-in-green or cast separately and laminated. The number of sintering steps involved thus depends mostly on the manufacturing sequence of the half-cell. There are a minimum of three (half-cell + barrier + air electrode) or a maximum of five sintering steps if the support and fuel electrode are sintered separately or at least one calcination step is applied. For special applications (requirement of extremely high performance or very low overall operating temperature < 650°C), the replacement of some screen-printed layers with thin (< 1 µm) layers applied using physical vapor deposition methods (PVD) can lead to a noticeable reduction in cell resistance and, therefore, higher performance at given operational conditions. A prerequisite for thin electrolytes and/or barrier layers are extremely smooth surfaces that need to be coated. In particular, the coating of a PVD-8YSZ on the porous fuel electrode is challenging, as the layer thickness of the electrolyte reaches the structural dimensions of the electrode (pore/grain size).

MSC

From a manufacturing perspective, metal-supported cells are particularly different from the two types mentioned above. All functional layers have to be deposited on a thick, extremely coarse metal substrate, which typically exhibit either large grain sizes (20–150 µm) or simply laser-drilled holes in a flat metal sheet. The base metals used are Fe-Cr ferritic steels with some minor additions ensuring creep resistance, corrosion resistance (bearing in mind that water vapor pressure can reach 100%, especially in electrolysis mode), and the formation of a conductive and well-adhering oxide scale (chromia or Cr-containing spinels). Ideally, the metal support and the material used for the metallic interconnects (see next paragraph) should be similar. When manufacturing MSCs, it must also be considered that none of the coating techniques require a sintering step at high temperatures and in ambient air, as this would severely destroy the metal support. Thin-film technologies such as PVD, electrophoretic deposition, and sputtering are therefore mostly used. The fuel electrode, which consists of Ni and GDC, can be applied by screen printing and – in contrast to ESCS/FESCs – metallic nickel can be used, as the subsequently applied sintering step can be performed in vacuum or in reducing conditions (e.g. H_2). As the fuel electrode is fine-grained, intermediate layers are also applied between the coarse support and the electrode. Typically, they have a roughly similar composition (Ni/GDC) but with particle size distributions lowered in a stepwise manner to avoid infiltration into the layer underneath. Due to the

interdiffusion of Ni from the electrode and Fe and Cr from the metal, a barrier layer is also applied (e.g. GDC) either by PVD/sputtering or screen printing. The materials for the electrolyte, the air-side barrier layer, and the air electrode are similar to ESCs/FESCs. The air electrode materials are prone to chemical deterioration when sintered in vacuum or reducing conditions, which is why they are usually not sintered but adhered in situ during cell/stack start-up. Some perovskite compositions deteriorate during reduced sintering but can be reconverted to the initial perovskite during the start of operation under ambient air [18].

Advantages/limitations of the aforementioned cell types

The main advantage of ESCs is the ability to change electrode compositions and microstructures, the relatively easy manufacturing sequence, and, therefore, the better scale-up possibilities with respect to size and production capacity. The main drawback of ESCs is the thick electrolyte, leading to high operation temperatures (≥ 800°C) due to its high ohmic resistance.

FESCs typically require greater manufacturing effort than ESCs but if the half-cell is tape cast green-in-green or laminated, the effort involved is the same. Due to the thick, porous support, strength and manageability is limited and the cell size is therefore also restricted. But the thin electrolyte leading to low ohmic resistance favors the FESC for operation at lower temperatures (600–700°C) by maintaining a high performance.

MSCs, which are still less mature than ESCs and FESCs, have the great advantage of material compatibility between the fuel-side support and the metallic interconnect, resulting in easier cell integration into the stack. Additionally, start-up times are shorter, as the metal has a better thermal conductivity and the cells are more robust due to the ductile support. Mobile and transportation applications might therefore be one favorable area of use. The main disadvantage is that the metallic support will degrade/corrode and operation temperatures are thus limited to below 650°C, which results in operation mostly with pure hydrogen.

Cell contact

To ensure good mechanical and electrical contact between the cell and the metallic interconnects (IC) on both sides of the cell, contact elements are incorporated. On the fuel side is a Ni mesh/felt/wrought and on the air side is a perovskite comparable to, or a material equivalent to, the used air electrode. In MSC stacks, the Ni mesh can be omitted if there is direct contact between the metal support and the IC and if the support can also act as a gas distributor within the fuel compartment. In ESC- and FESC-based stacks, the Ni mesh also assumes the gas distribution function, thus avoiding machining/structuring of the IC. The air-side contact material also ensures good contact by compensating for manufacturing tolerances and surface roughness and typically has a coarse structure to ensure good gas permeability.

Interconnects

In Figure 2, a principal cross section of one single repeating unit (SRU) is shown, representing one plane in a planar stack. The interconnects or bipolar plates have various functions: they connect all planes electronically, they separate the gas chambers, and they distribute the gas streams. According to the different planar cell types, two materials classes are used for ESCs and FESCs. Both metal classes are chosen in accordance with the overall coefficient of thermal expansion (CTE) of the cell. ESCs with a CTE dominated by the electrolyte mostly use CrFe5Y as an interconnect material. This alloy consists of ~ 94 wt % Cr, 5 % Fe, and ~ 1 % Y_2O_3 as a creep-enhancing addition. CrFe5Y forms a pure Cr_2O_3 oxide scale under water vapor and air conditions. For FESCs, typical alloys are high Cr-containing stainless steels. They are composed of 20–26 wt % Cr and some alloying elements which enhance oxide scale adhesion, enhance creep resistance, and, in particular, Mn is added to form a double-layered oxide scale. This oxide scale builds up an inner chromia layer and an outer Sr-Mn spinel layer, which reduces Cr evaporation from the interconnect. Industrial representatives are, for example, Crofer22APU and Crofer22H from VDM Metals and subsequently developed alloys with comparable compositions. Those

steels are adapted to the somewhat higher CTE of the FESC, which is dominated by its Ni/YSZ support. MSCs use the same alloy for the IC as for the metallic support of the cells.

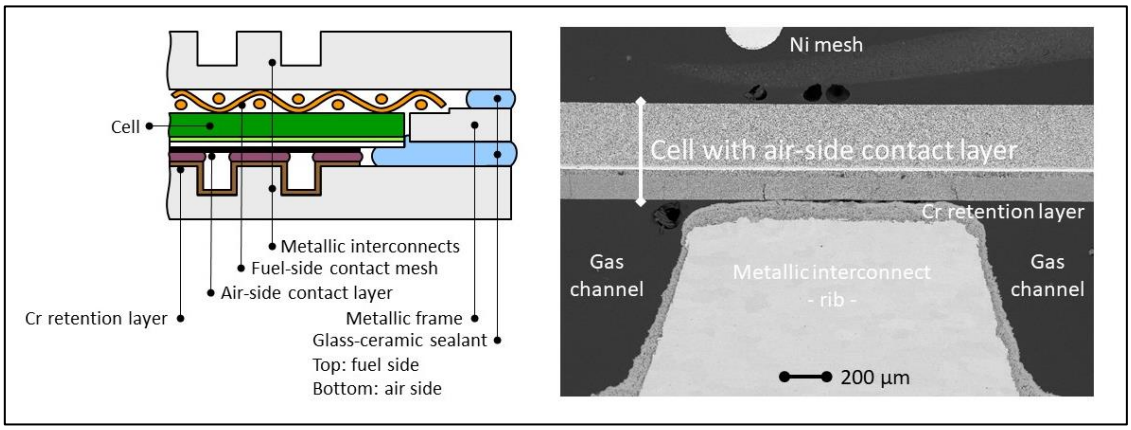

Figure 2: Left: schematic cross section of an SOC single repeating unit; right: cross section of a Jülich F-type short stack (SEM; polished surface)

Sealants

Gas-tight sealants are necessary in two regions within one SRU (see Figure 2). The first one seals the fuel gas compartments to the outside and the second one seals the cell into the metallic frame. Fundamental requirements for sealants include stability against oxidizing and reducing conditions, electronic insulation, compatibility with the metal interconnect and the cell materials, gas tightness, and robustness with respect to, for example, thermal cycling. At present, glass-ceramic sealants based on earthen alkali alumina-boro-silicate glasses are mostly used. They are typically applied by dispensing a paste or printing them on the ICs. During stack heat-up, the binder evaporates and the particles are transformed into a glass followed by an annealing step to partly crystallize the glass. Glass-ceramics are superior to glasses, as their mechanical behavior is better and their chemical stability is higher. Disadvantages of glass-ceramics include the often long crystallization phase to ensure the right crystals. This hinders a quick manufacturing process and set-up and means that the stack is a rigid block after sealing, thus limiting easy dismantling, SRU replacement, and recycling possibilities [19].

As an alternative, dismantlable sealant materials such as mica plates are sometimes used. They can be integrated either between the stack and the system as an adapter (allowing a quick stack change) or within the stack between specific areas, for example stacks with an open air side do not need to be gas-tight between the air compartment and the surrounding area.

3. Stack

3.1 Design

Two main families of SOC stack designs are currently in use: the tubular design and the more common planar stack design. As mentioned in section 2, we focus on the planar design in this article. All three main cell architectures (ESC, FESC, and MSC) are available in planar form and can be employed. Due to varying sizes, thicknesses, and performance, a concrete stack design is often optimized for a specific cell architecture, although some designs have the flexibility to accommodate FESC or ESCs with small adjustments. Figure 3 shows two planar stack designs developed and used by Forschungszentrum Jülich GmbH: the F10 design with one cell (10 cm by 10 cm FESC with 80 cm² active area) per repeating unit and the H20 design with four such cells in a “window frame” layout per repeating unit. F10 stacks are mainly a platform for research and development, while the H20 offers greater power per stack volume and footprint with up to 120 repeating units per stack. They can be used in fuel cell mode, electrolysis mode (steam and co-electrolysis of steam and carbon dioxide), and reversible mode. Both stacks mainly use the high-temperature steel Crofer22APU with a protective coating (MCF, $MnCo_{1.9}Fe_{0.1}O_4$), nickel

meshes for contact with the fuel electrode and gas distribution on the fuel side, screen-printed green foils of glass-ceramic sealants, and an internal (closed) air manifold.

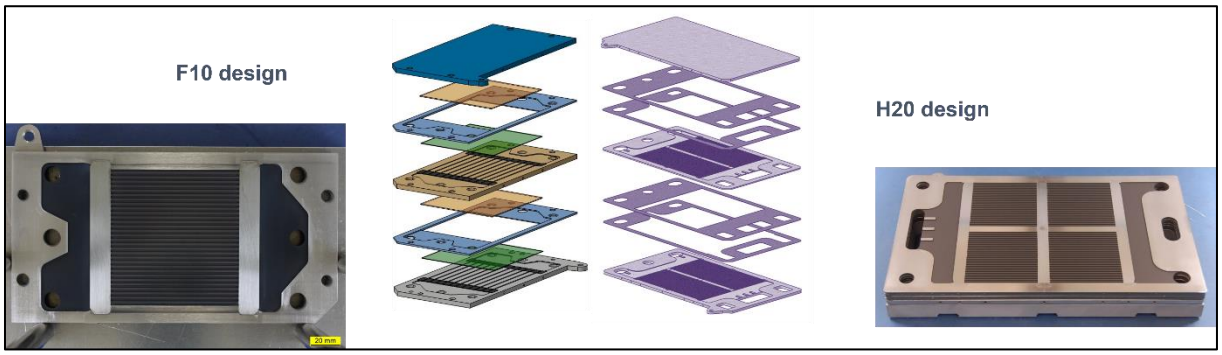

Figure 3: F10 (left) and H20 (right) stack designs of Forschungszentrum Jülich GmbH. Cells for the F10 are depicted in green, cell frames in light blue, and interconnects and nickel meshes in orange.

In SOC stacks, the air flux not only supplies the oxidant (O_2 in fuel cell mode) but is also used to cool the stack during operation, as the fuel cell-related chemical reactions are exothermic. Operating cells with high current densities (high power density) requires a sufficiently high air flux to remove the residual heat. One aspect in developing a stack is to design the air side (manifold and flow field) in such a way as to maintain low pressure losses at the required air flows and to also ensure a low differential pressure between the air side and the fuel side in order to minimize stress on the cells and structural materials of the stack. Depending on the operation mode, different flow schemes are used to optimize heat distribution in the stack: a) co-flow in which fuel and air flow in parallel through the stack, b) counter flow in which both gases enter the stack at opposite sides, and c) cross flow in which both gas streams are perpendicular to each other. Besides the internal air manifolds employed in the F10 and H20 designs, external (open) air manifolds are very common due to their flexibility. With this approach, the air side of the cells is open to the stack environment. Examples for such designs include the CFY design of Fraunhofer IKTS [4], the SMK-B230 design of Sunfire GmbH [1], and the E3000 design of Elcogen AS [12]. The fuel side is always designed as a closed manifold.

3.2 Electrochemical characterization techniques

i-V curves

The most common characterization technique is the measurement of a polarization (i-V) curve. With this method, a current ramp is applied to the stack and the voltage response of the stack, individual cells, and groups of cells is measured. The voltage is usually plotted versus the applied current density and fuel utilization (in FC mode; or conversion ratio in the general case), although many specialized variants exist. The current density is defined as the applied current divided by the optical active area visible on the air side and is given in Acm^{-2} values. An example of a polarization curve in fuel cell mode with dry hydrogen as a fuel is shown in Figure 4 (left), which shows the voltage of the cell (layer) 2 and the temperature vs. the current density at three different starting stack temperatures. In this example, the i-V is not recorded isothermally, i.e. the heat released by the electrochemical reaction changes the stack temperature during the measurement. This needs to be taken into account when comparing i-V curves.

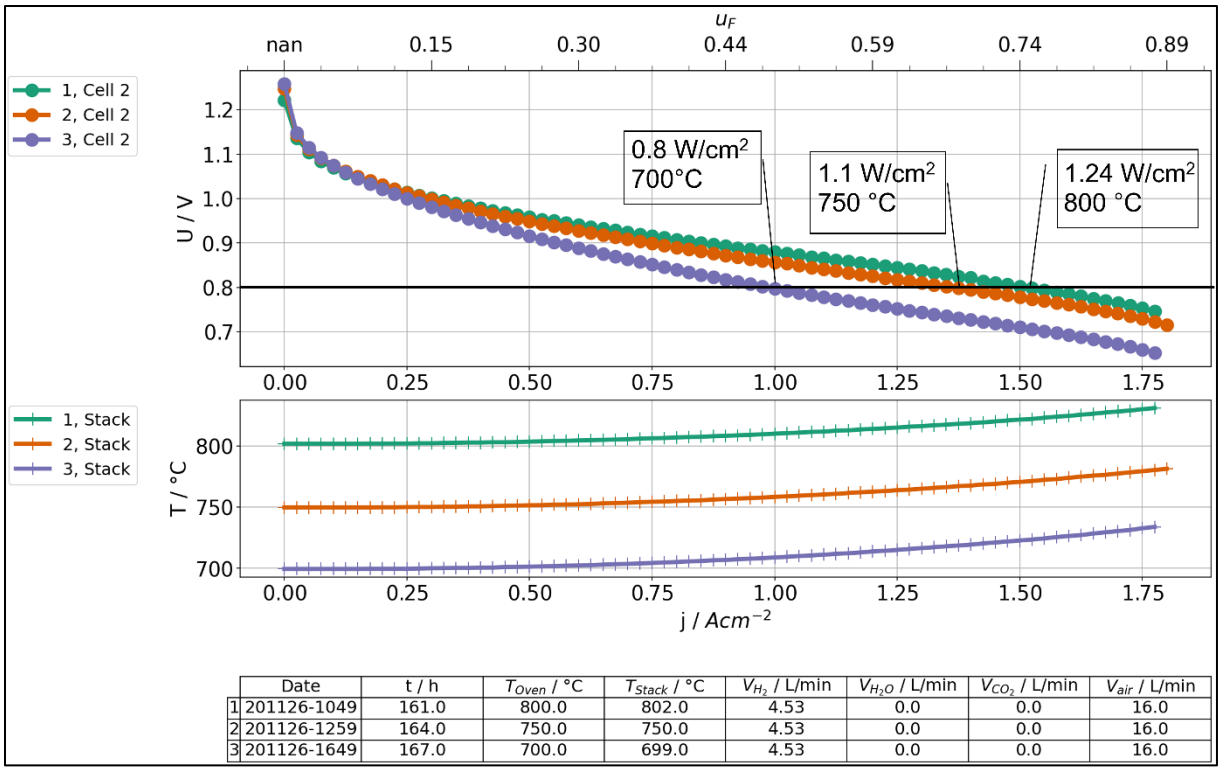

	Date	t / h	T_{Oven} / °C	T_{Stack} / °C	V_{H_2} / L/min	V_{H_2O} / L/min	V_{CO_2} / L/min	V_{air} / L/min
1	201126-1049	161.0	800.0	802.0	4.53	0.0	0.0	16.0
2	201126-1259	164.0	750.0	750.0	4.53	0.0	0.0	16.0
3	201126-1649	167.0	700.0	699.0	4.53	0.0	0.0	16.0

Figure 4: Polarization curve for an F10 stack in fuel cell mode with dry hydrogen as a fuel (left). Stationary co-electrolysis in an F10 stack showing cell voltages of layers 2 and 3, stack temperature, stack current, and stack voltage vs. operation time (right).

The voltage response reveals a lot of information. The first point (at zero current) is the open circuit voltage (OCV). When measured in dry hydrogen, this OCV is heavily influenced by traces of humidity. A leakage of the cell or the sealing of the stack thus often reduces it with respect to the theoretical value that can be calculated using the Nernst equation. This serves as one quick diagnostic criterion to check the gas-tightness of the unit. The region with an exponential change of cell voltage exhibits a Butler–Volmer-like activation behavior of the cell, but this effect is very small at high temperatures and is overshadowed by a change of the Nernst potential in the fuel electrode caused by the water released by the reaction. At higher current densities, the i-V curve shows a wide, quasi-linear section, which is heavily determined by the electrolyte and contact resistances. At high levels of fuel utilization, a mass transport (or diffusion) limitation effect takes hold and leads to a steep drop in cell voltages, as the remaining fuel available for the reaction becomes very low. The example in Figure 4 barely shows this effect, showing good gas supply and distribution even at 90% utilization. There are a few aspects to bear in mind when recording and evaluating i-V curves on the stack level. Firstly, it is not a single cell that is measured, but rather the cell within its environment (the stack) with its thermal inertia, gas distribution characteristics, and contact situation. In addition, while polarization curves allow a simple way of determining the cell current or cell power at a given cell voltage, they are strongly dependent on the operation parameters (gas flows, temperature, current sweep rate, etc.). This is important when comparing i-V curves and a given point on the curve does not necessarily correspond to the behavior at the same stationary operation conditions. The measurement is only possible “offline”, i.e. not during stationary operation. And lastly, the measurement of polarization curves is not necessarily nondestructive and might change cells or other components in the stack.

Operation at reference conditions

The “gold standard” for measuring stack degradation is still to operate the stack at a suitable reference condition and to record the deterioration of cell voltage (or power, resistance, etc.) over time. An example of this approach can be seen in Figure 4 (right), which shows a stationary co-electrolysis operation of a mixture of 60% steam, 30% carbon dioxide, and 10% hydrogen in an F10 stack at 750°C with an applied current of 1 A cm^{-2} and a conversion rate of 70%. After a break-in period, the cell voltage degradation assumes a constant rate, which can then be linearly fitted and estimated. However, a simple

extrapolation of the degradation rate into the (far) future should be avoided, since degradation mechanisms (and therefore rates) can change over time. In this way, several thousand hours can typically be monitored, with the longest running SOC test in public knowledge lasting approx. 100,000 hours. Accelerated tests would be very useful and help to reduce costs, but the general problem of accelerating degradation speed while ensuring that degradation mechanisms remain unchanged has not yet been solved [20]. There are, however, specific accelerated tests in use, for example when adding harmful substances to the gas flows.

AC-based techniques

Besides traditional direct-current-based polarization techniques, there are a range of alternating-current-based techniques, with electrochemical impedance spectroscopy (EIS) being the most popular. Here, a sinusoidal perturbation is modulated onto the DC current through the stack. Through phase-sensitive measurements of the resulting cell voltage excitations, the transformation into the frequency domains, and subsequent mathematical analysis, the contributions of individual processes (e.g. diffusion processes and charge-transfer processes) can be resolved. In most cases, a deconvolution of the obtained spectra by equivalent circuit modeling or by estimating the distribution of relaxation times is necessary. This method is a particularly useful tool for monitoring degradation over time and attributing degradation causes. Fig. 5 shows an example of such a spectrum and deconvolution with the attribution of some important processes [21-23].

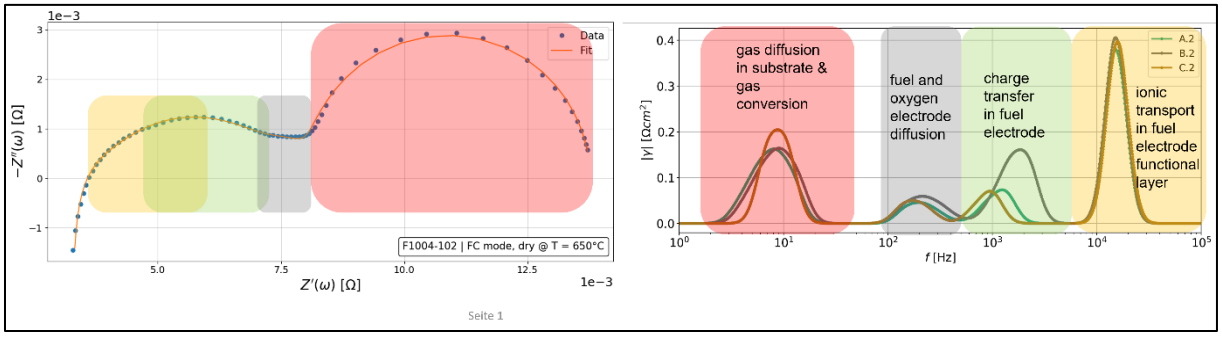

Figure 5: EIS spectrum of an SOC in an F10 stack in fuel cell mode in dry hydrogen at 650°C (left) and deconvolution of the spectrum by estimating DRT (right). Assumed frequency ranges for some important processes in the cell are indicated by color.

3.3 Prominent degradation effects

Two prominent degradation effects are interconnect oxidation and chromium poisoning. Over time, steels form oxide scales consisting mainly of chromium oxide at operation conditions, which may result in additional voltage losses. Moreover, under the given atmospheric conditions, chromium forms volatile species and poisons the air electrode through the formation of insulating phases such as $SrCrO_4$ [24]. To reduce both effects, specially designed high-temperature ferritic stainless steels like Crofer22 (1.4760 X1CrTiLa22) [25] combined with protective coatings on the interconnects (e.g. MCF, $MnCo_{1.9}Fe_{0.1}O_4$) are employed. The coatings can be applied by wet powder spraying (WPS), inkjet printing [26], or atmospheric plasma spraying (APS), which produce a much denser coating [27-29]. Recent modelling showed that in the case of APS-MCF on Crofer22APU, the share of overall degradation due to interconnect oxidation dropped below 1% [30] while long-term experiments also showed that chromium evaporation was reduced very efficiently [31]. To optimize costs, another approach is to combine a less resistant material with a suitable protective coating alone, for example the Sanergy HT 441 employs an AISI 441 substrate with a Ce/Co coating applied by physical vapour deposition (PVD) [32].

On the fuel side, the migration of nickel remains an unsolved degradation phenomenon. In particular, in the case of FESCs with a Ni/YSZ electrode in electrolysis mode, active nickel particles in the functional layer next to the YSZ electrolyte are lost due to the migration of nickel away from the electrolyte into the substrate layer. This firstly causes a loss of electrocatalytically active triple phase boundary points (where electron conductor, ion conductor, and pore meet) and, secondly, an effective increase in

thickness of the electrolyte, thus causing an additional ohmic resistance. The underlying mechanism is still a subject of discussion but one prominent hypothesis points to the surface diffusion of $Ni(OH)_x$ species at typical operation conditions [33]. The issue seems to be less severe for ESCs based on Ni/GDC electrodes, but it remains an obstacle for commercialization.

4. System

The system design for SOECs differs from that of AFCs and PEECs. The most important difference is thermal management and the requirement of SOECs to have only gaseous media, i.e. steam instead of liquid water. While low-temperature electrolysis stacks require cooling to operate at a stable temperature, an SOEC system typically requires additional heaters to heat the inlet gases or the stack directly. The heaters are required, on the one hand, to heat up the system to operation temperature and, on the other hand, to provide heat to compensate for losses, mainly caused by the hot off-gas. Depending on the cell type and operation temperature of the SOEC, additional heat is required to support the endothermal electrolysis reaction. For an industrial process, in the case of either off-heat and/or off water vapor are available, the heaters can be adapted in size and the overall SOEC efficiency increases substantially.

Figure 6 shows a typical SOEC system design. A steam generator generates steam from feed water. The steam generator is usually electrically powered, while a smaller fraction of the energy required for evaporation can be recovered from the off-gas [34, 35]. Steam and air preheaters are important for efficiency to recover most of the energy from the hot gases exiting the stack. To supply additional heat to the stack, electrical gas heaters (as shown in Figure 6) can be used or the stack can be heated by integrated heating plates [36, 37]. For small stacks, heat can also be supplied from the outer stack surface [38]. A supply of air to the stack reduces the efficiency by about 1.5 % [34], but it prevents potential hazards due to concentrated oxygen at high temperatures. Furthermore, it contributes to lower temperature gradients inside the stack in combination with gas heaters. Most new systems are designed like this. An overview of newly built SOEC systems with published details was recently presented [35].

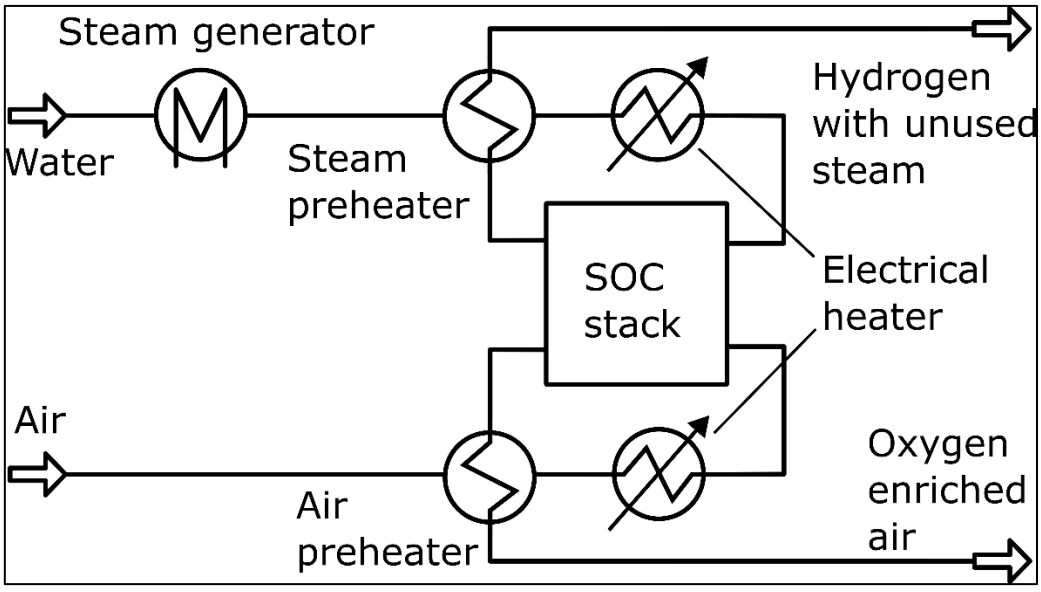

Figure 6. A typical SOEC system design

Cell performance has no direct impact on system efficiency for electrolysis. While ohmic and transport losses in the SOC reduce efficiency during fuel cell operation, for electrolysis it only shifts power from the heaters to the stack and has no effect on the total input power or production rate. The efficiency of an SOEC system can thus be characterized by its loss of energy to the environment. Figure 7 shows an overview of the major loss contributions for the electrolysis operation of a recently built system [37].

The figure shows the losses for operation at 80 % steam utilization and a current density of 1 $A \cdot cm^{-2}$. The data exclude AC-DC conversion losses.

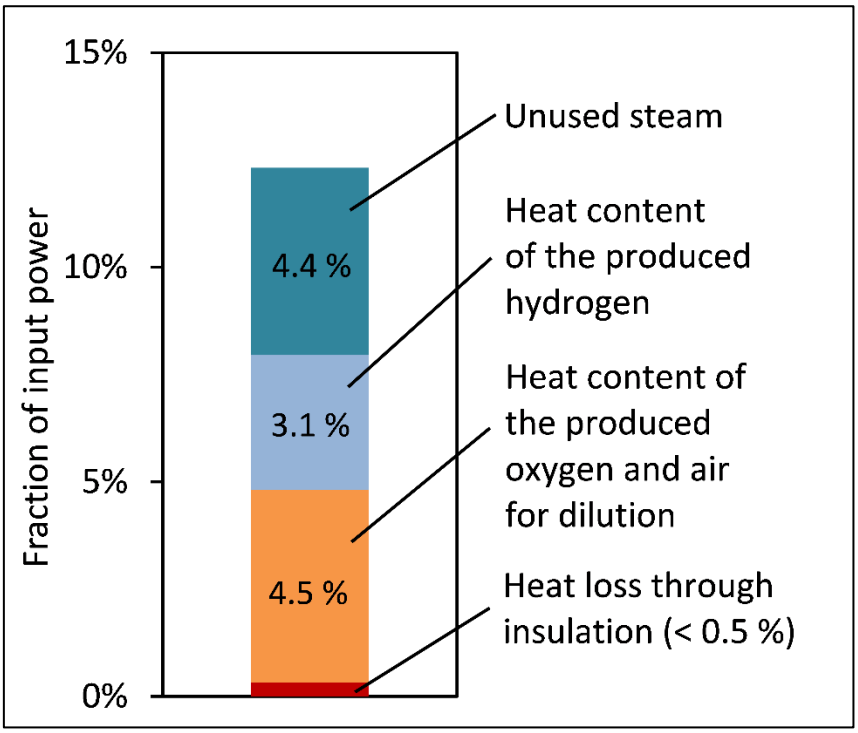

Figure 7. Typical losses for SOC electrolysis in relation to input power

SOEC systems used for operation with CO_2 or CO_2/steam mixtures (co-electrolysis) instead of pure steam are designed in a similar way. The main difference is the smaller or missing steam generator and measures to prevent the formation of elemental carbon. These measures (e.g. quenching of the off-gas) can reduce system efficiency due to the limited heat recovery options. As suggested by the GrInHy research project, the steel industry might in future provide excess steam, which can be used for SOECs [39, 40].

When integrated in larger processes, SOEC systems can benefit from externally provided heat. In the case of steam electrolysis, the heat is typically used to generate steam at atmospheric pressure and thus replaces electricity for the electric boiler. One example of such a process is the production of synthetic alcohols as fuels or educts for the chemical industry. The heat released by the exothermic formation of alcohol from syngas can be utilized for steam generation.

In theory, SOEC systems can also benefit from externally provided high-temperature heat to the stack due to the endothermal characteristic of the electrolysis reaction [41]. In practice, however, applications with heat available at 700°C and higher are rare and complex to handle. However, it has been experimentally demonstrated to provide high-temperature heat for SOECs by solar power [42].

5. Conclusion

Solid oxide cell systems either for fuel cell mode or electrolysis mode are market-ready and many companies have started to offer systems for various applications and sizes. Those systems are based on all three types of planar cells: electrolyte-, fuel-electrode-, and metal-supported cells. Most of the cell- and stack-related materials have been developed in the last two decades in terms of chemistry and microstructure and operate well – at least in the medium term (~ 10,000–40,000 h). Degradation rates in fuel cell mode have reached values below 0.5 %/1000 h and those for electrolysis mode are in the range of around 1–2 %/1000 h.

Various planar stack designs are in use today, supporting the different cell architectures. While designs may be optimized for specific operational modes, most designs enable operation in fuel cell mode, electrolysis mode, and reversible mode. Common challenges are to ensure proper cell contact, durable sealing of the stacks while preventing short-circuits, and heat management. Interconnect oxidation and chromium evaporation do not pose a severe risk today thanks to the application of suitable protective coatings. Proven techniques for performance characterization and diagnosis exist, but attributing specific damage during operation and predicting a remaining useful lifetime remain challenging. Obtaining reliable information on the durability of a given stack still requires extensive and expensive long-term testing.

The intensive global efforts for at least a partially hydrogen-based future energy landscape is now also driving SOC technology. In particular, the integration of an SOC system into high-temperature processes enables extremely high electrical and thermal efficiencies, thus reducing the cost factor, which still plays an important role. Besides scaling up, enhancing reproducibility, and reducing costs, initial ideas have been developed to integrate SOCs into a circular economy, including recycling possibilities and strategies. Together with low-temperature fuel cell and electrolyzer systems, SOCs will certainly play a key role in the future global energy system.

6. References

[1] https://www.sunfire.de/de/; accessed on Nov. 29th 2022

[2] http://www.hexis.ch/; accessed on Nov. 29th 2022

[3] https://www.bloomenergy.com/; accessed on Nov. 29th 2022

[4] https://www.ikts.fraunhofer.de/en/departments/energy_systems/materials_and_components/ceramic_energy_converters.html and other sub-sites of IKTS; accessed on Nov. 29th 2022

[5] https://www.kerafol.com/sofc; accessed on Nov. 29th 2022

[6] https://www.ceres.tech/; accessed on Nov. 29th 2022

[7] https://www.bosch-sofc.com/de/; accessed on Nov. 29th 2022

[8] https://en.weichaipower.com/about/sustainability/we_are_in_action/201808/t20180814_43280.html; accessed on Nov. 29th 2022

[9] https://www.doosanfuelcell.com/en#scrollSkip; accessed on Nov. 29th 2022

[10] https://www.avl.com/all-press-releases; Press release: avl-and-ceres-set-to-combine-competencies-for-solid-oxide-fuel-cell-systems-technology; accessed on Nov. 29th 2022

[11] https://solydera.com/; accessed on Nov. 29th 2022

[12] https://elcogen.com/; accessed on Nov. 29th 2022

[13] https://nexceris.com/; accessed on Nov. 29th 2022

[14] https://ssc-energy.dtu.dk/; accessed on Nov. 29th 2022

[15] De Haart L.G.J., Beale S.B., Deja R., Dittrich L., Duyster T., Fang Q., Foit S., Groß-Barsnick S.-M., de Haart U., Hoven I., Kruse N., Lenser C., Ma Q., Margaritis N., Menzler N.H., Naumenko D., Nohl M., Peters Ro., Sebold D., Thaler F., Tiedemann W., Unachukwu I.D., Varghese B., Vibhu V., Vinke I.C., Wolf S., Zhang S., Zurek J. and Blum L.: Forschungszentrum Jülich – Current activities in SOC development. ECS Trans. 103 (2021), 299-306

[16] Blum L., Fang Q., de Haart L.G.J., Malzbender J., Margaritis N., Menzler N.H., Peters R.: Progress in SOC development at the Forschungszentrum Jülich. 14th European SOFC & SOE Forum 2020. A0501, A sessions, 88-96

[17] Udomsilp D., Rechberger J., Neubauer R., Bischof C., Thaler F., Schafbauer W., Menzler N. H., de Haart L., Nenning A., Opitz A. K., Guillon O., Bram M.: Metal-supported solid oxide fuel cells with exceptionally high power density for range extender systems. Cell Rep. Phys. Sci. 1 (2020), 100072

[18] Udomsilp D., Thaler F., Menzler N.H., Bischof C., de Haart L.G.J., Opitz, K.A., Guillon O., Bram M.: Dual-phase cathodes for metal-supported solid oxide fuel cells – Processing, performance, durability. J. Electrochem. Soc. 166/8 (2019), F506-F510

[19] Sarner S., Schreiber A., Menzler N.H., Guillon O.: Recycling strategies for solid oxide fuel and electrolyzer cells. Adv. Energy Mat. 12 (2022), 2201805 (1-19)

[20] Blum L., Fang Q., Groß-Barsnick S.-M., de Haart L.G.J., Malzbender J., Menzler N.H., Quadakkers W.J.: Long-term operation of solid oxide fuel cells and preliminary findings on accelerated testing. Int. J. Hydrogen En. 45 (2020), 8955-8964
[21] Caliandro P., Nakajo A., Diethelm S., Van herle J.: Model-assisted identification of solid oxide cell elementary processes by electrochemical impedance spectroscopy measurements. J. Power Sources 436 (2019), 226838
[22] Weber A., Szász1 J., Dierickx S., Endler-Schuck C., Ivers-Tiffée E.: Accelerated Lifetime Tests for SOFCs. ECS Trans. 68 (2015), 1953
[23] Leonide A., Rüger B., Weber A., Meulenberg W.A., Ivers-Tiffée E.: Impedance study of alternative (La,Sr)$FeO_{3-\delta}$ and (La,Sr)(Fe,Co)$O_{3-\delta}$ MIEC cathode compositions. J. Electrochem. Soc. 157 (2010), B234-B239
[24] Konysheva E., Penkalla H., Wessel E., Mertens J., Seeling U., Singheiser L., Hilpert K.. J. Electrochem. Soc. 153 (2006), A765-A773
[25] https://www.vdm-metals.com/fileadmin/user_upload/Downloads/Data_Sheets/Data_Sheet_VDM_Crofer_22_APU.pdf; accessed on Feb. 24th 2023
[26] Pandiyan S., El-Kharouf A., Steinberger-Wilckens R.: Formulation of spinel based inkjet inks for protective layer coatings in SOFC interconnects. J. Colloid and Interface Sci. 579 (2020), 82-95
[27] Vaßen R., Grünwald N., Marcano D., Menzler N.H., Mücke R., Sebold D., Sohn Y.J., Guillon O.: Aging of atmospherically plasma sprayed chromium evaporation barriers. Surface and Coatings Technol. 29 (2016), 115-122
[28] Grünwald N., Sebold D., Sohn Y.-J., Menzler N.H., Vaßen R.: Self-healing atmospheric plasma sprayed $Mn_{1.0}Co_{1.9}Fe_{0.1}O_4$ protective interconnector coatings for solid oxide fuel cells. J. Power Sources 363 (2017), 185-192
[29] Grünwald N., Y.J. Sohn, X. Yin, Menzler N.H., Guillon O., Vaßen R.: Microstructure and phase evolution of atmospheric plasma sprayed Mn-Co-Fe oxide protection layers for solid oxide fuel cells. J. Europ. Ceram. Soc. 39 (2-3) (2019), 449-460
[30] Yu S., Zhang S., Schäfer D., Peters R., Kunz F., Eichel R.A.: Numerical modelling and simulation of the solid oxide cell stacks and metal interconnect oxidation with OpenFOAM. *Energies* (2023, submitted)
[31] Fang Q., Menzler N.H., Blum L.: Degradation analysis of long-term solid oxide fuel cell stacks with respect to chromium poisoning in $La_{0.58}Sr_{0.4}Co_{0.2}Fe_{0.8}O_{3-\delta}$ and $La_{0.6}Sr_{0.4}CoO_{3-\delta}$ cathodes. J. Electrochem. Soc. 168 (2021), 104505
[32] https://www.alleima.com/en/products/coated-strip-steel/sanergy-ht/; visited on Feb. 24th 2023
[33] Mogensen M.B., Chen M., Frandsen H.L., Hauch A., Hendriksen P.V., Jacobsen T., Jensen S.H., Skafte T.L.,Sun X.: Ni migration in solid oxide cell electrodes: Review and revised hypothesis. Fuel Cells 21 (2021), 415-429
[34] Kruse N., Tiedemann W., Hoven I., Deja R., Peters Ro., Blum L., Peters Ra.: Experimental investigation of efficiency maximization in solid oxide electrolysis systems by internal steam and heat recovery. ECS Trans. 103 (2021), 555–560
[35] Min G., Choi S., Hong J.: A review of solid oxide steam-electrolysis cell systems: Thermodynamics and thermal integration. Applied Energy Bd. 328 (2022), 120145
[36] Peters Ro., Frank M., Tiedemann W., Hoven I., Deja R., Kruse N., Fang Q., Blum L., Peters R.: Long-term experience with a 5/15kW-class reversible solid oxide cell system. J. Electrochem. Soc. 168 (2021) 014508
[37] Peters Ro., Tiedemann W., Hoven I., Deja R., Kruse N., Fang Q., Blum L., Peters Ra.: Development of a 10/40kW-class reversible solid oxide cell system at Forschungszentrum Jülich. ECS Trans. 103 (2021) 289–297
[38] Saarinen V., Pennanen J., Kotisaari M., Thomann O., Himanen O., Iorio S. D., Hanoux P., Aicart J., Couturier K., Sun X., Chen M., Sudireddy B.R.: Design, manufacturing, and operation of movable 2 × 10 kW size rSOC system. Fuel Cells (2021) 477–487
[39] Posdziech O., Schwarze K., Brabandt, J.: Efficient hydrogen production for industry and electricity storage via high-temperature electrolysis. Int. J. Hydrogen En. 44 (2019), 19089–101
[40] Posdziech O., Geißler T., Schwarze K., Blumentritt R.: System development and demonstration of large-scale high-temperature electrolysis. ECS Trans. 91 (2019), 2537–46

[41] Peters Ro., Deja R., Blum L., Nguyen V.N., Fang Q., Stolten D.: Influence of operating parameters on overall system efficiencies using solid oxide electrolysis technology. Int. J. Hydrogen En. 40 (2015), 7103–7113
[42] Schiller G., Lang M., Szabo P., Monnerie N., von Storch H., Reinhold J., Sundarraj P.: Solar heat integrated solid oxide steam electrolysis for highly efficient hydrogen production. J. Power Sources 416 (2019), 72–78